

Role of stable modes in zonal flow regulated turbulence

K. D. Makwana, P. W. Terry, and J.-H. Kim

Citation: *Phys. Plasmas* **19**, 062310 (2012); doi: 10.1063/1.4729906

View online: <http://dx.doi.org/10.1063/1.4729906>

View Table of Contents: <http://pop.aip.org/resource/1/PHPAEN/v19/i6>

Published by the [American Institute of Physics](#).

Related Articles

The q-profile effect on high-order harmonic q=1 tearing mode generation during sawtooth crashes
Phys. Plasmas **19**, 062108 (2012)

Aspect ratio effects on neoclassical tearing modes from comparison between DIII-D and National Spherical Torus Experiment
Phys. Plasmas **19**, 062506 (2012)

Rapid filamentation of high power lasers at the quarter critical surface
Phys. Plasmas **19**, 063112 (2012)

Development of a stable dielectric-barrier discharge enhanced laminar plasma jet generated at atmospheric pressure
Appl. Phys. Lett. **100**, 253505 (2012)

High sensitivity, low noise Mirnov coil array on Prairie View rotamak
Rev. Sci. Instrum. **83**, 10E304 (2012)

Additional information on *Phys. Plasmas*

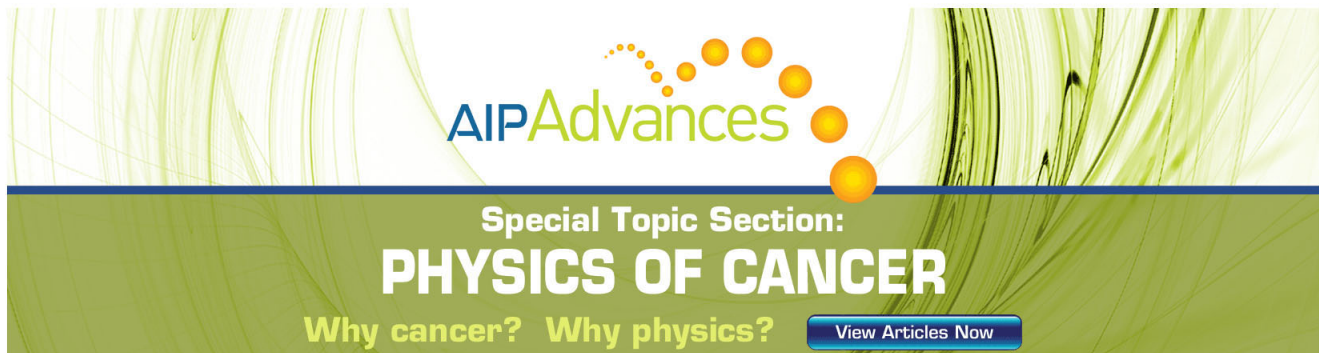
Journal Homepage: <http://pop.aip.org/>

Journal Information: http://pop.aip.org/about/about_the_journal

Top downloads: http://pop.aip.org/features/most_downloaded

Information for Authors: <http://pop.aip.org/authors>

ADVERTISEMENT



AIP Advances

Special Topic Section:
PHYSICS OF CANCER

Why cancer? Why physics? [View Articles Now](#)

Role of stable modes in zonal flow regulated turbulence

K. D. Makwana, P. W. Terry, and J.-H. Kim

Department of Physics, University of Wisconsin-Madison, Madison, Wisconsin 53706, USA

(Received 16 January 2012; accepted 20 May 2012; published online 29 June 2012)

Zonal flows are shown to regulate ion temperature gradient turbulence by enabling efficient energy transfer from the instability to a damped eigenmode in the unstable wavenumber range. The damped mode also saturates turbulence when zonal flows are not active in saturation dynamics, for example, in electron temperature gradient turbulence, but the transfer from unstable to stable mode is less efficient and requires a larger amplitude to balance the instability drive. From numerical solutions of a fluid model with a single damped eigenmode, an eigenmode decomposition of the nonlinear evolution shows that the dominant energy transfer involves the triplet correlation of the unstable mode, the zonal flow, and the stable mode at three wavenumbers satisfying $k = k' + k''$. In this triplet, nearly all of the energy from the instability goes to the damped mode. The very small fraction going to the zonal flow is balanced by small zonal flow damping. This combination of unstable mode, zonal flow, and stable mode minimizes the nonlinear frequency mismatch and avails itself of large coupling strengths associated with the zonal flow. © 2012 American Institute of Physics. [<http://dx.doi.org/10.1063/1.4729906>]

I. INTRODUCTION

Recently, it has been found that damped modes are important energy sinks in the saturation of many types of instability-driven plasma turbulence.^{1–3} These modes are zeros of the linear dispersion relation with negative growth rate. They can be represented by fluctuation decompositions, including proper orthogonal decomposition.⁴ Two features of the damped modes are striking: (1) they robustly damp fluctuation energy at the same scales as the instability, typically in the large scale range where the turbulent spectrum peaks and (2) nonlinearity, in the form of three-wave coupling, drives all damped modes available to the system.⁵ In two-field fluid models, there is one damped mode and one unstable mode, both of which are functions of wavenumber from large to small scales.¹ In gyrokinetics there are in principle an infinite number of damped modes spanning directions of inhomogeneity in phase space. Under numerical discretization, the number becomes finite but very large [$O(10^4)$ for typical resolutions].³ Whether the number of damped modes is one or many, certain aspects of the saturation are qualitatively the same. Damped modes dissipate energy at a rate that is comparable to the rate of energy injected by the instability. The dissipation peaks in the same wavenumber range as the instability. If the damped modes are artificially removed, the saturation level increases by at least an order of magnitude.⁶ This set of features has been observed for a diverse collection of turbulent systems.¹ One of the most widely studied systems is ion temperature gradient (ITG) turbulence, where the above described features have been found in two- and three-field fluid systems^{1,5,7} and gyrokinetic representations.³

ITG turbulence is known to involve zonal flows in its saturation.^{8,9} When the coupling to zonal flows is artificially suppressed, fluctuation levels increase significantly, typically by an order of magnitude.¹⁰ The reason for this effect is

typically held to be the suppressive effect of flow shear.^{11,12} Shearing is an aspect of advection, which is inertial and unable to dissipate energy directly. Rather, shearing enhances inertial energy transfer to small scales,¹³ which are thought to have stronger collisional dissipation. Although this can and does help in saturation of ITG, dissipation by damped modes can be a much more important factor in the energy balance of saturation. Damped modes remove energy from the turbulence in two ways. First, they drive a negative heat flux, putting energy back into the temperature gradient. Second, they remove energy through the viscous and diffusive dissipation terms. The first effect, which counters the outward heat flux driven by the linear instability, is not irreversible. The second effect is. However, since both remove energy from the fluctuations, both will be referred to as “energy dissipation by stable eigenmodes.” Also, the words “stable modes” and “damped modes” will be used interchangeably. Dissipation due to damped modes is strongest in the large-scale range where instability growth rates are largest.³ Damped eigenmodes in this range remove most of the energy injected by the instability and saturate it, making transfer to high k a secondary player in saturation physics. Damped eigenmodes have not been accounted for in describing the effect of zonal flows on ITG turbulence. Likewise, the description of the saturation of ITG turbulence by damped modes has not studied the role of zonal flows in saturation.¹ This paper investigates the interaction of zonal flows and damped modes in the saturation of ITG turbulence.

We explicitly track nonlinear energy transfer between all types of fluctuations in a simple model for ITG turbulence introduced by Holland *et al.*¹⁴ The fluctuations include the linearly unstable eigenmode, the linearly stable eigenmode, a zonal flow ($ik_x\phi_{k_y=0}$ where ϕ is the electrostatic potential), and a zonal pressure (the $k_y = 0$ component of the pressure). Nonlinear energy transfer rates between these components

can be measured in numerical simulations. The energy transfer channels are sufficiently simple and transparent to allow a clear picture of what happens in saturation. Similar analysis for gyrokinetics is under way and will be reported elsewhere.

The saturation of the instability has two distinct stages. In the first, the linearly unstable mode pumps both zonal fields (pressure and flow) and the damped eigenmode by a parametric instability process.⁶ Zonal fields and damped eigenmodes grow at a rate that is independent of their amplitudes. The growth rate is effectively the sum of the linear growth rates of two beating wavenumbers of the unstable mode in the region of fastest linear growth. This mechanism is only efficient when the fastest growing mode dominates the spectrum, and when the amplitudes of the damped mode and zonal fields are small. Later, when these conditions are not met, phase mixing between a larger number of unstable modes at different wavenumbers and damped modes reduces the efficiency of this energy transfer channel. At this point, the second saturation stage takes over. With the zonal flow and pressure at finite amplitude, a triplet interaction of the unstable mode, the stable mode, and either of the zonal fields is found to have the smallest triplet complex frequency of any of the three-wave combinations possible. The result is a very long nonlinear interaction time and a highly efficient energy transfer channel from the unstable mode to the stable mode, via the zonal fields. The coupling coefficients of interactions with the zonal flow are larger than those with zonal pressure, with the amplitudes of zonal pressure and zonal flow being comparable. In the triplet interaction of the unstable mode, the zonal flow, and the stable mode, virtually all of the energy passing from the unstable mode is deposited on the stable mode, with less than 1% deposited on the zonal flow. Weak collisional damping easily balances the small amount of energy deposited into the zonal flow, providing saturation of the zonal flow. The first saturation stage corresponds to the large overshoot of fluctuation level typically observed in simulations.^{15,16} The second stage is the time-asymptotic saturated state. The process described above is distinct from the shearing mechanism, as evident in the minimum complex frequency condition that characterizes the dominant energy transfer channel. With this mechanism, the zonal flow instead acts as a catalyst through its nonlinear frequency to allow very efficient large-scale energy transfer from the instability to the damped eigenmode.

This paper is organized as follows. Section II describes the model, the decomposition into linear eigenmodes and zonal fields, and the coupling coefficients in the decomposition. In Sec. III numerical solutions are presented. Section IV discusses the triplet frequency, coupling coefficients, zonal field amplitudes, and their role in the dominant energy transfer channel. Conclusions are given in Sec. V.

II. TWO-FIELD ITG MODEL AND STABLE MODE ANALYSIS

We study a 2D two-field fluid model that describes both ITG and electron temperature gradient (ETG) turbulence.¹⁴ The equations are

$$\begin{aligned} \frac{\partial p_k}{\partial t} + ik_y(1 + \eta)\phi_k + \chi k^4 p_k \\ = -\frac{1}{2} \sum_{k'} (k' \times \hat{z} \cdot k) [\phi_{k'} p_{k-k'} - \phi_{k-k'} p_{k'}], \end{aligned} \quad (1)$$

$$\begin{aligned} [\delta(k_y) + k^2] \frac{\partial \phi_k}{\partial t} + ik_y \phi_k - ik_y \epsilon p_k + \nu k^2 \phi_k \\ = -\frac{1}{2} \sum_{k'} (k' \times \hat{z} \cdot k) [(k - k')^2 - k'^2] \phi_{k'} \phi_{k-k'}, \end{aligned} \quad (2)$$

where p_k and ϕ_k are Fourier amplitudes of pressure and electrostatic potential, ν and χ are coefficients of collisional dissipation, η is the ratio of density to temperature gradient scale lengths, and ϵ is the ratio of density gradient scale length to magnetic field variation scale length. The spatial coordinates are normalized to ρ and time is normalized to L_{ref}/u_{ref} . The symbol ρ represents the electron gyroradius for the ETG turbulence case and the ion sound gyroradius for the ITG turbulence case. The symbol L_{ref} represents the density gradient scale length and u_{ref} is v_{Te} for ETG and c_s for ITG. To set the model for ETG turbulence, $\delta = 1$ for all k_y . For ITG,

$$\delta(k_y) = \begin{cases} 1 & \text{if } k_y \neq 0 \\ 0 & \text{if } k_y = 0. \end{cases}$$

Poloidally symmetric $k_y = 0$ fluctuations are referred to as zonal fields. In this model, there are two zonal fields, namely, the zonal flow $v_z(k_x) = ik_x \phi_{k_y=0}$ and the zonal pressure $p_{k_y=0}$. There is a zonal flow and pressure for both the ETG and ITG cases. In the ITG case where $\delta(k_y)|_{k_y=0} = 0$, the potential equation can be rewritten as an equation for zonal flow

$$\dot{v}_z + \nu v_z = (-i/2) \sum_{k'} k'_y [(k_x - k'_x)^2 - k'^2] \phi_{k'} \phi_{k-k'}. \quad (3)$$

In the ETG case the equation for v_z is

$$\begin{aligned} \dot{v}_z + \nu k_x^2 (1 + k_x^2)^{-1} v_z = (-i/2) \sum_{k'} k'_y k_x^2 (1 + k_x^2)^{-1} \\ \times [(k_x - k'_x)^2 - k'^2] \phi_{k'} \phi_{k-k'}. \end{aligned} \quad (4)$$

For the energy containing scales $k_x \ll 1$. Thus, the nonlinear coupling to the zonal flow is stronger by a factor k_x^{-2} in the ITG case than in its ETG counterpart. Since transfer to $k_y = 0$ is already favored when damped eigenmodes are present,¹⁷ the zonal flow is strongly excited. The zonal flow brings down the level of turbulence and reduces ion-channel transport. This is shown in Fig. 1, where the turbulent energy in the ITG case is almost two orders of magnitude smaller than the ETG case. The definition of energy is given later.

The linear dispersion relation yields two eigenfrequencies given by

$$\begin{aligned} \omega_{1,2} = -\frac{i}{2} \left(\chi k^4 + \frac{\nu k^2 + ik_y}{\delta + k^2} \right) \\ \pm \frac{i}{2} \left\{ \left(\chi k^4 - \frac{\nu k^2 + ik_y}{\delta + k^2} \right)^2 + \frac{4(1 + \eta)k_y^2 \epsilon}{\delta + k^2} \right\}^{1/2}. \end{aligned} \quad (5)$$

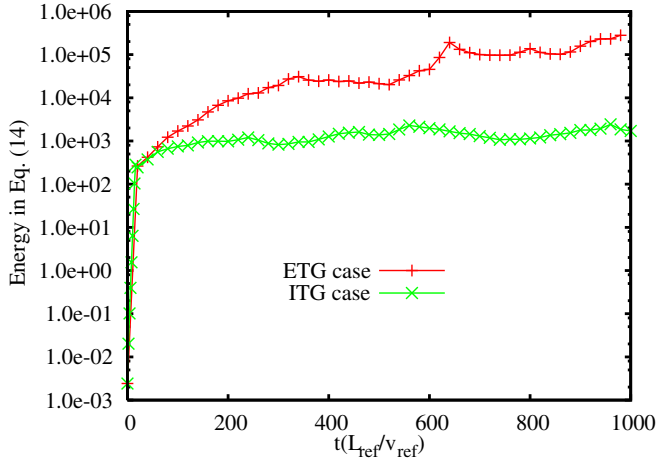


FIG. 1. The total turbulent energy in the ITG case is significantly reduced compared to the ETG case.

We consider the regime of weak collisionality $\chi k^4, \nu k^2 \ll k_y \sqrt{\eta \epsilon}$, where $0 < k_y < 1$. This is a regime of robust linear instability. In this regime, an expansion of the radical shows that the two eigenfrequencies are nearly complex conjugates, with the deviation proportional to the collisionalities,

$$\omega_{1,2} \approx \frac{k_y}{2(\delta + k^2)} \pm ik_y \left[\frac{(1 + \eta)\epsilon}{\delta + k^2} \right]^{1/2} - \frac{i}{2} \frac{\nu k^2}{(\delta + k^2)} - \frac{i}{2} \chi k^4. \quad (6)$$

As a near conjugate to the unstable eigenmode ω_1 , the second eigenmode ω_2 is damped. Moreover, with $|\text{Im } \omega_2| \approx |\text{Im } \omega_1|$, the damped eigenmode satisfies the condition for strong excitation⁵ and dissipates energy at a rate that is comparable to the energy injection rate of the instability.¹ For $k_y = 0$, the eigenfrequencies reduce to

$$\omega_1 = -i\nu k_x^2 / (\delta + k_x^2), \quad (7)$$

$$\omega_2 = -i\chi k_x^4. \quad (8)$$

We observe from Eqs. (1) and (2) that setting $k_y = 0$ diagonalizes the linear part of the equations. Hence pressure and potential are the eigenmodes at $k_y = 0$. (Away from $k_y = 0$, the eigenmodes are linear combinations of pressure and potential given below.) For convenience, we label the frequencies of the $k_y = 0$ flow and pressure as, respectively, ω_1 and ω_2 , irrespective of whether $(\chi k_x^4 - \nu k_x^2 / (\delta + k_x^2))$ is positive or negative. This is a labeling convention for $k_y = 0$ and does not change the results of this paper in any way. For the ITG case, the zonal flow damping rate is $-\nu$.

To track the amplitudes of the unstable and damped modes, we introduce the eigenmode decomposition,¹

$$\begin{pmatrix} p_k \\ \phi_k \end{pmatrix} = \beta_1(k) \begin{pmatrix} R_1(k) \\ 1 \end{pmatrix} + \beta_2(k) \begin{pmatrix} R_2(k) \\ 1 \end{pmatrix}, \quad (9)$$

where $[R_1(k), 1]$ and $[R_2(k), 1]$ are the eigenvectors of the unstable and stable modes, $\beta_1(k)$ and $\beta_2(k)$ are the mode amplitudes, and

$$R_{1,2} = \frac{-\omega_{1,2}(\delta + k^2) + k_y - i\nu k^2}{k_y \epsilon}. \quad (10)$$

Evolution equations for the amplitudes $\beta_1(k)$ and $\beta_2(k)$ are found by inverting Eq. (9) and taking the time derivative.⁵ This procedure diagonalizes the linear coupling of the evolution equations, while mixing the nonlinearities.

It is helpful to explicitly break out the $k_y = 0$ component of the evolution from the $k_y \neq 0$ components, writing the evolution equations as two equations for $\dot{\beta}_1(k)|_{k_y \neq 0}$ and $\dot{\beta}_2(k)|_{k_y \neq 0}$ and two equations for $\dot{p}_k|_{k_y=0}$ and $\dot{\phi}_k|_{k_y=0}$. The evolution equations are

$$\begin{aligned} \dot{\beta}_l + i\omega_l \beta_l &= \sum_{k'_y (k'_y \neq 0, k_y)} [C_{lmn} \beta'_m \beta''_n] \\ &+ \sum_{k'_x} \{ [C_{lFn} v'_z \beta''_n + C_{lPn} p'_z \beta''_n] |_{k'_y=0} \\ &+ [C_{lFm} \beta'_m v''_z + C_{lPm} \beta'_m p''_z] |_{k'_y=k_y} \}, \end{aligned} \quad (11)$$

$$\dot{v}_z + \frac{\nu k_x^2}{(\delta + k_x^2)} v_z = \sum_{k'_x} [C_{Fmn} \beta'_m \beta''_n] |_{k_y=0}, \quad (12)$$

$$\dot{p}_z + \chi k_x^4 p_z = \sum_{k'_x} [C_{Pmn} \beta'_m \beta''_n] |_{k_y=0}, \quad (13)$$

where $l, m, n = 1$ or 2 and the Einstein convention is used to imply summation over repeated indices. A shorthand notation is introduced as follows: $\beta_{1,2} = \beta_{1,2}(k)|_{k_y \neq 0}$, $\beta'_{1,2} = \beta_{1,2}(k')|_{k'_y \neq 0}$, $\beta''_{1,2} = \beta_{1,2}(k - k')|_{k'_y \neq k_y}$, $v_z = ik_x \phi_k|_{k_y=0}$, $v'_z = ik'_x \phi_{k'}$, $v''_z = i(k_x - k'_x) \phi_{k-k'}|_{k'_y=k_y}$, $p_z = p_k|_{k_y=0}$, $p'_z = p_{k'}|_{k'_y=0}$, and $p''_z = p_{k-k'}|_{k'_y=k_y}$. The coupling coefficients C_{lmn} , C_{lFn} , C_{lPn} , C_{lFm} , C_{lPm} , C_{Fmn} , and C_{Pmn} are functions of the nonlinear coefficients of Eqs. (1) and (2) and the eigenvector components R_1 and R_2 . Their precise forms are given in the Appendix.

Equations (11)–(13) can be recast as energy equations by multiplying by β_l^* , v_z^* , and p_z^* , respectively, and adding the complex conjugate equations. Energy transfer channels available to the system are associated with various coupling coefficients. Turbulent energy enters the system through $|\beta_1|^2$ at low k , and energy transfer channels lead from this source to the sinks, the largest of which is $|\beta_2|^2$ at low k . $|\beta_1|^2$ and $|\beta_2|^2$ at high k are also sinks, but energy must cascade through a progression of wavenumbers to reach large k . Energy passes directly from β_1 to β_2 , without any intermediate zonal fields, through terms with coefficients C_{112} , C_{121} , C_{122} , C_{211} , C_{212} , and C_{221} . Energy cascades to large k within a single eigenmode branch through the terms with C_{111} and C_{222} . The terms with C_{1F2} , C_{12F} , C_{2F1} , C_{21F} , C_{F12} , and C_{F21} govern the passage of energy from β_1 to β_2 through the intermediary of the zonal flow. The terms with C_{1P2} , C_{12P} , C_{2P1} , C_{21P} , C_{P12} , and C_{P21} govern the passage of energy from β_1 to β_2 through the zonal pressure. The relative strengths of these channels are governed by the magnitudes of coupling coefficients and by the triplet correlations of the energy equations, as detailed in Sec. IV.

III. ENERGY TRANSFER TO STABLE MODES VIA ZONAL FLOWS

To examine nonlinear energy transfer, we introduce the energy, defined as,

$$E = \sum_k [(\delta + k^2)|\phi_k|^2 + |p_k|^2]. \quad (14)$$

The rate of change of the total energy can be expressed as

$$\frac{dE}{dt} = Q_u + Q_s + Q_{us} + D + D_{zonal}, \quad (15)$$

where Q_u is the rate of change of energy due to unstable modes, Q_s is the rate of energy removed by stable modes, and Q_{us} is the rate of change of energy due to cross terms of unstable and stable modes. The sum of these terms is related to the turbulent heat transport flux by $Q_u + Q_s + Q_{us} = -(1 + \eta + \epsilon)Q$, where $Q = -\sum_k k_y \text{Im}(\phi_k^* p_k)$ is the heat flux. D is high-wavenumber dissipation for nonzonal modes, and D_{zonal} is the linear energy damping rate of the zonal modes. These terms can be derived by substituting Eqs. (1) and (2) in the time derivative of Eq. (14). They are given in the Appendix. These quantities are plotted in Fig. 2 for the ETG case. We see that Q_u is large and positive. It is balanced by a large and negative Q_s , which shows saturation by stable modes. Q_{us} is small (not visible in the plot) and negative, and helps balance Q_u . It should be noted that while Q_{us} equally derives from stable and unstable modes, it vanishes in any calculation that ignores the stable modes. The role of viscous dissipation D is considerably smaller than the dissipation Q_s of stable modes, and dissipation by the zonal modes is negligible. The ETG turbulence in Fig. 2 has not actually saturated at the end of the simulation run. While the addition of artificial damping at low k does lead to saturation, the behavior seen in Fig. 2 ($Q_u \sim |Q_s| \gg |Q_{us}|, D$) remains unchanged.

A numerical experiment shows how zonal flows reduce the level of turbulence. A simulation is started in the ETG case. It is allowed to reach a saturated state. At time 400, the

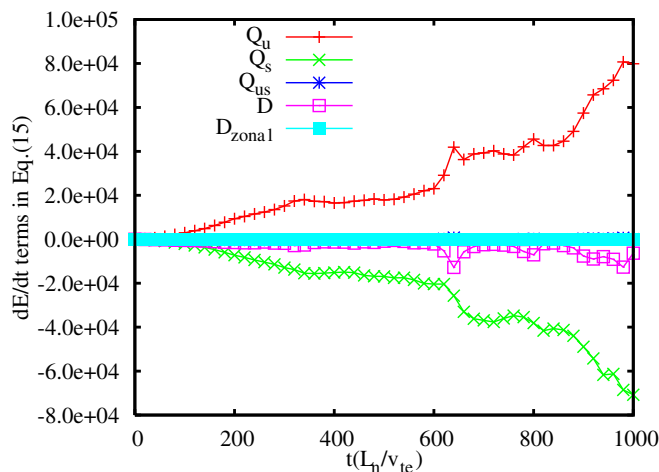


FIG. 2. The rate of change of energy in the ETG case, divided into various components as defined in Eq. (15).

equations are switched to the ITG case by changing the parameter δ . In some sense, this mimics a transition from a low confinement regime to a high confinement regime induced by turbulence-driven sheared flows.^{14,18} The turbulence level is reduced after $t = 400$. What causes this change in energy? The rate of change of energy, dE/dt , becomes sharply negative after $t = 400$. We see from Eq. (15) that dE/dt has a net drive from $Q_u + Q_s + Q_{us}$ and net dissipation $D + D_{zonal}$. Fig. 3 shows that as zonal flows are turned on, the viscous dissipation D shows only a slight transient increase and then a decrease. The zonal dissipation D_{zonal} remains small. However, the sum $Q_u + Q_s + Q_{us}$ decreases drastically in magnitude. The sum $Q_u + Q_s + Q_{us}$ is the difference between energy injected by the instability and dissipated by damped modes. This residual must be dissipated by the only other sink, namely, viscous dissipation. Consequently viscous dissipation does not increase (the way it would if there were enhanced energy transfer to small scale) but it decreases to match the reduced residual energy input $Q_u + Q_s + Q_{us}$. The reduced input makes dE/dt negative and brings the energy down. It is also observed that the level of zonal flows increases. However, the fraction of instability energy deposited into the zonal flow remains very small and is removed by zonal flow damping, as shown in Fig. 4. This figure shows that most of the instability energy is damped by the stable modes, with the zonal flow acting as a crucial mediator for the energy transfer from unstable to stable modes.

Decomposing the pressure and potential fields into the linear eigenmode amplitudes, the energy dependence on the four fields of Eqs. (11)–(13) is given by

$$E = \sum_{k_y \neq 0} [(1 + k^2 + |R_1|^2)|\beta_1|^2 + (1 + k^2 + |R_2|^2)|\beta_2|^2 + 2(1 + k^2)\text{Re}(\beta_1^* \beta_2) + 2\text{Re}(R_1^* \beta_1^* R_2 \beta_2)] + \sum_{k_y=0} [|p_k|^2 + (\delta + k^2)|\phi_k|^2]. \quad (16)$$

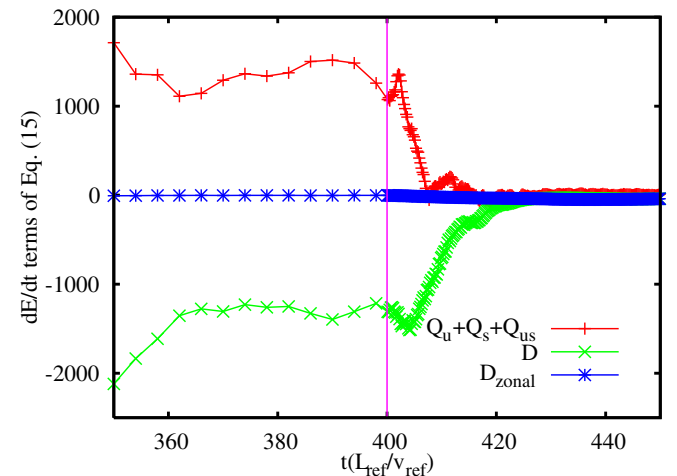


FIG. 3. The net heat flux (drive) $Q_u + Q_s + Q_{us}$, the high k dissipation D , and the dissipation at zonal wavenumbers D_{zonal} when the zonal flows are “turned on” at time $t = 400$. The zonal flows are turned on by changing $\delta_{k_y=0}$ from 1 to 0.

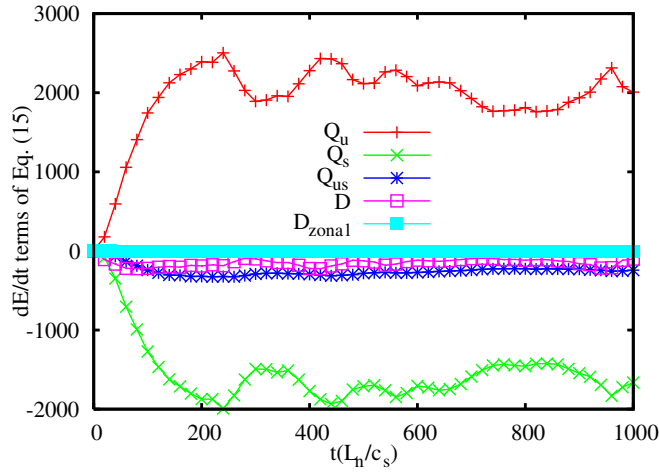


FIG. 4. The rate of change of energy in the ITG case, divided into various components as defined in Eq. (15).

The energy in the unstable modes corresponds to $\sum_{k_y \neq 0} (1 + k^2 + |R_1|^2) |\beta_1|^2$. Taking a derivative and substituting from Eq. (11), the rate of change of energy of the unstable modes is

$$\begin{aligned} & \frac{\partial}{\partial t} \left[\sum_{k_y \neq 0} (1 + k^2 + |R_1|^2) |\beta_1|^2 \right] \\ &= \left[\sum_{k_y \neq 0} 2(1 + k^2 + |R_1|^2) \gamma_1 |\beta_1|^2 \right] + N_{111} + N_{112} + N_{121} \\ & \quad + N_{122} + N_{1P1} + N_{1P2} + N_{11P} + N_{12P} + N_{1F1} \\ & \quad + N_{1F2} + N_{11F} + N_{12F}. \end{aligned} \quad (17)$$

The term $\gamma_1 |\beta_1|^2$ is the linear instability energy input rate, where γ_1 is the growth rate of the unstable mode. The terms labelled by N represent the three wave coupling terms. Their forms are given in the Appendix. The term N_{111} signifies coupling between the unstable mode $\beta_1(k)$ with two other unstable modes at k' and k'' . The terms N_{112} and N_{121} represent coupling of the unstable mode with another unstable and one stable mode. The term N_{122} represents coupling of the unstable mode with two stable modes. The remaining terms N_{11P} , N_{1P1} , N_{12P} , N_{1P2} , N_{1F1} , N_{11F} , N_{1F2} , and N_{12F} are couplings of the unstable mode with a zonal field (zonal pressure or zonal flow) and a second mode, either unstable or stable. These last eight terms can be grouped together as coupling of the unstable mode with a zonal field and either a stable or unstable mode. The four groups of coupling terms just described are plotted in Fig. 5, which shows both the ETG and ITG cases. The curve labelled $\gamma_1 |\beta_1|^2$ is the linear energy injection rate ($\sum_{k_y \neq 0} 2(1 + k^2 + |R_1|^2) \gamma_1 |\beta_1|^2$). It is balanced by the nonlinear energy transfer terms. In the ETG case, all four groups of nonlinear terms play approximately equal roles in saturating the linear instability. In the ITG case, the group involving couplings with a zonal field is the most important term for saturation of the instability. This indicates that zonal fields play a prominent role in saturating turbulence in the case of ITG. The zonal fields include both

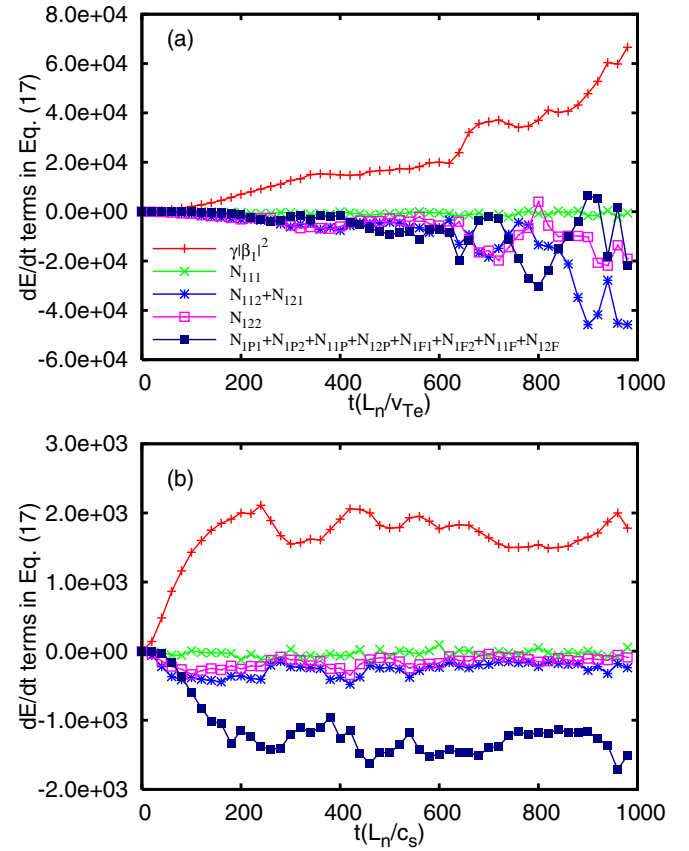


FIG. 5. The rate of change of the unstable mode energy, $\sum_{k_y \neq 0} (1 + k^2 + |R_1|^2) d|\beta_1|^2/dt$, divided into the various coupling terms as a function of time. (a) is for ETG case and (b) is for ITG case. The legend is the same for both plots.

zonal pressure and zonal flow, so it is important to ask what role each field individually plays in saturation. Also, in the couplings with a zonal field, only one mode of the triad is a zonal field, the other mode being either a stable or an unstable nonzonal mode. Hence, it is important to ask about the proportion of energy transferred to the zonal field compared to the energy transferred to the nonzonal mode.

To answer these questions, we separate the group involving one zonal field into four subgroups. They are couplings with (1) zonal pressure and an unstable mode ($N_{11P} + N_{1P1}$), (2) zonal pressure and a stable mode ($N_{12P} + N_{1P2}$), (3) zonal flow and an unstable mode ($N_{11F} + N_{1F1}$), and (4) zonal flow and a stable mode ($N_{1F2} + N_{12F}$). These terms are plotted in Fig. 6. This figure is for the ITG case, where the zonal field coupling terms are the most important. Two sets of nonlinear terms dominate. The first is the coupling between the unstable mode at k , a zonal flow, and a second unstable mode ($N_{11F} + N_{1F1}$). This term is positive, which means that energy is flowing into unstable modes from this term. Since this energy transfer is summed over all nonzonal wavenumbers, the net transfer of energy between the unstable mode at k and the unstable mode at either k' or k'' should cancel out. Consequently, the energy transfer $N_{11F} + N_{1F1}$ is coming entirely from the zonal flow. For comparison with other transfer rates, we note that $N_{11F} + N_{1F1}$ has a value of approximately 1900 at time $t = 400$. The second dominant set of nonlinear terms represents coupling with a zonal flow

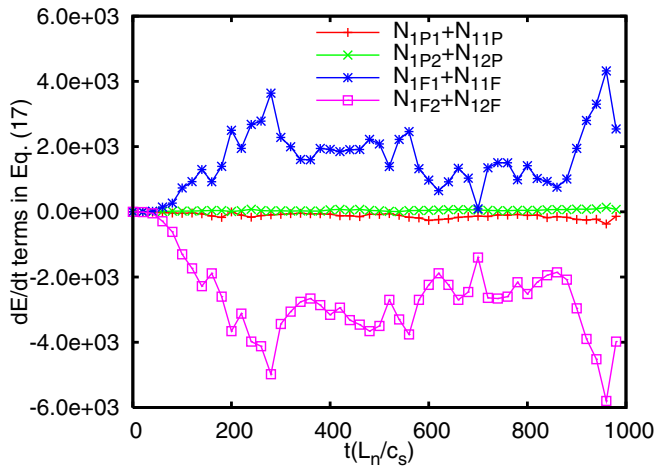


FIG. 6. The zonal field couplings of the unstable mode energy in ITG case.

and a stable mode ($N_{12F} + N_{1F2}$). This set of terms has a value of -3100 at $t=400$, making it larger than $N_{11F} + N_{1F1}$ and negative. This means that this energy transfer is going out of the unstable modes. Some portion of this energy transfer goes into zonal flows. This portion is necessarily larger than $N_{11F} + N_{1F1}$ because, as we will see later, the zonal flow receives net energy from the unstable mode. The energy transfer $N_{11F} + N_{1F1}$ thus recirculates within the unstable mode, through the intermediary of the zonal flow. The remainder of the energy transfer $N_{12F} + N_{1F2}$ from the unstable mode goes into stable modes.

These transfers are depicted schematically in Fig. 7(a). The transfer $N_{11F} + N_{1F1}$ is represented by an arrow flowing into the unstable modes from the zonal flow. The portion of

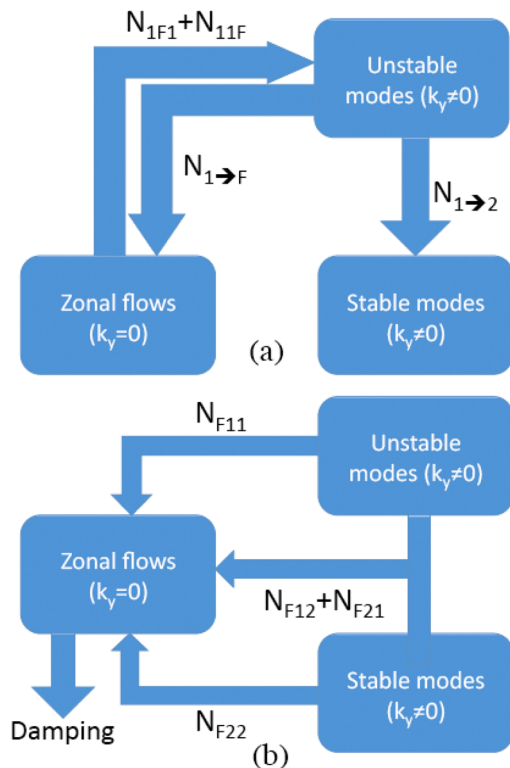


FIG. 7. A cartoon showing the nonlinear energy transfer rates for the unstable mode (a) and the zonal flow (b).

$N_{12F} + N_{1F2}$ that goes into zonal flows is represented by $N_{1\rightarrow F}$. The portion that flows into the stable modes is represented by $N_{1\rightarrow 2}$. $N_{1\rightarrow F}$ and $N_{1\rightarrow 2}$ are taken as positive quantities. Therefore, the portions $N_{1\rightarrow F} + N_{1\rightarrow 2}$ add up to $-N_{12F} - N_{1F2}$. It is not possible to determine $N_{1\rightarrow F}$ and $N_{1\rightarrow 2}$ separately from this information alone. To estimate them, we need to look at the energy dynamics of the zonal flow. The energy equations for the zonal fields are (for ITG case)

$$\sum_{k_y=0} \frac{\partial}{\partial t} (|p_k|^2) = \left[\sum_{k_y=0} -2\chi k^4 |p_k|^2 \right] + N_{P11} + N_{P12} + N_{P21} + N_{P22}, \tag{18}$$

$$\sum_{k_x=0} \frac{\partial}{\partial t} (k_x^2 |\phi_k|^2) = \left[\sum_{k_x=0} -2\nu k_x^2 |\phi_k|^2 \right] + N_{F11} + N_{F12} + N_{F21} + N_{F22}. \tag{19}$$

The terms containing χ and ν represent linear damping of the zonal pressure and flow, respectively. The terms labelled N are again the various nonlinear couplings of the zonal fields, which couple only with nonzonal wavenumbers. Following the usual notation, $N_{P(F)1(2)1(2)}$ represents coupling of the zonal pressure (flow) with an unstable (stable) mode at k' and an unstable (stable) mode at $k-k'$. These terms, which are given in the Appendix, are plotted in Fig. 8.

The dynamics of the zonal pressure shows that it receives energy from unstable modes through N_{P11} and saturates by transferring the energy to stable modes through

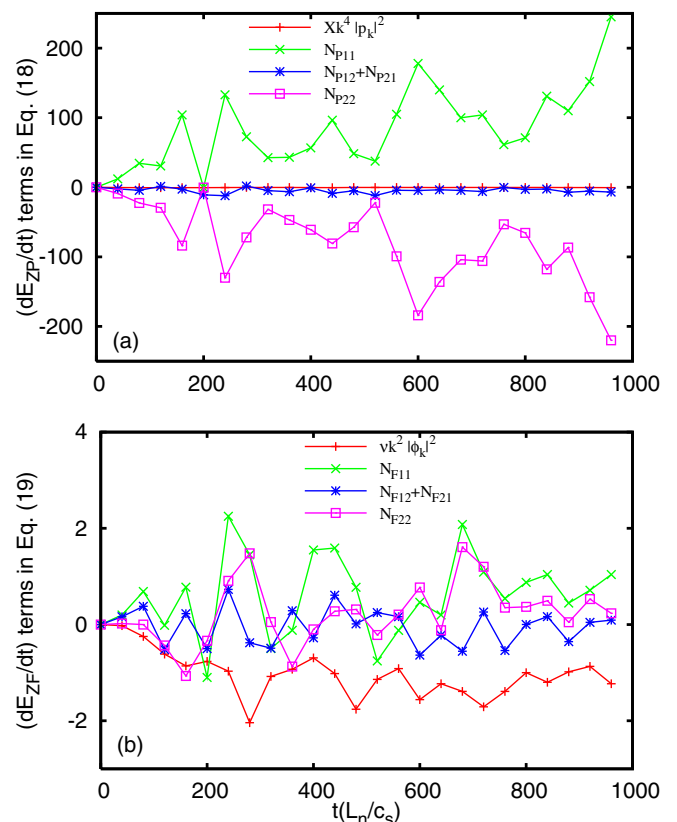


FIG. 8. The rate of change of energy terms for the zonal pressure (a) and zonal flow (b) for ITG case.

N_{P22} . The linear damping of zonal pressure plays a small role in its energetics. However, the zonal flow dynamics shows a strikingly different balance. The zonal flow receives energy equally from unstable modes through N_{F11} and stable modes through $N_{F12} + N_{F21}$ and N_{F22} , with saturation provided by its linear damping. This is schematically shown in Fig. 7(b). All the nonlinear terms N_{F11} , $N_{F12} + N_{F21}$, and N_{F22} are shown to be supplying energy to the zonal flow, with only linear damping providing saturation. The energy transfer to zonal flows is also seen to be much smaller than the transfer to zonal pressure. The y axis scale of Fig. 8(b) can be compared to that of Fig. 6. We see that the net transfer into the zonal flow from unstable mode (N_{F11}) is approximately only 2, compared to a value of 1900 for energy transfer from zonal flow to unstable mode ($N_{1F1} + N_{11F}$) at $t = 400$.

Looking at Fig. 7, we can say that $N_{F11} = N_{1 \rightarrow F} - (N_{1F1} + N_{11F})$. Since $N_{F11} \ll (N_{1F1} + N_{11F})$ from the above comparison, we can conclude that $N_{1 \rightarrow F}$ only exceeds $N_{1F1} + N_{11F}$ by a quantity of order 1, i.e., by 0.1%. Given that $-(N_{12F} + N_{1F2}) = N_{1 \rightarrow F} + N_{1 \rightarrow 2}$ and that $N_{1 \rightarrow F}$ is within 0.1% of $N_{1F1} + N_{11F}$, we can further say that $N_{1 \rightarrow 2} \approx -(N_{12F} + N_{1F2} + N_{1F1} + N_{11F})$ within a percent. This is shown in Fig. 9. This figure shows that N_{111} , $N_{112} + N_{121}$, N_{122} , and $N_{1P1} + N_{1P2} + N_{11P} + N_{12P}$ are small, and that $N_{1F1} + N_{11F} + N_{1F2} + N_{12F}$, which is equal to $N_{1F1} + N_{11F} - |N_{1F2} + N_{12F}| \approx -N_{1 \rightarrow 2}$, is the only significant net energy transfer term for the unstable-mode energetics with a value of -1250 at $t = 400$. Recall that $N_{1 \rightarrow 2}$ was defined as the energy transferred from the unstable to stable mode via three wave couplings that have a zonal flow as the third term in the interaction triplet. Thus, the net energy transfer dynamics in the equation for $|\beta_1|^2$ is dominated by transfer to the damped eigenmode, with zonal flows acting as a mediator, or a catalyst, of energy transfer from the unstable to stable mode.

The energy transfer rates just described, including the small rates N_{F11} and equivalent differences of large rates like $N_{1 \rightarrow F} - (N_{1F1} + N_{11F})$, are well outside the putative error bars associated with numerical effects that break energy conservation. Observing energy dynamics with growth

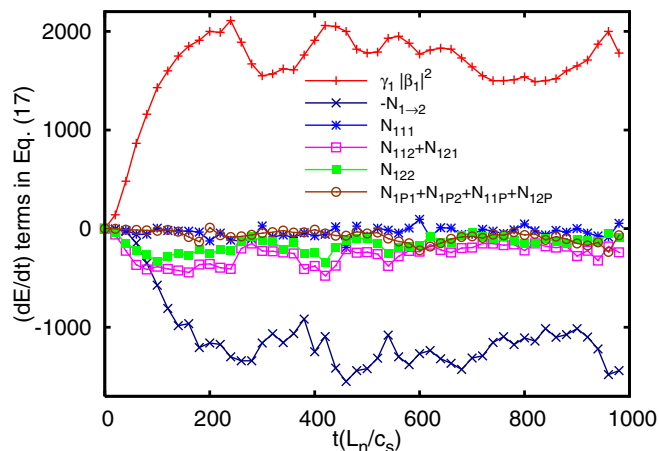


FIG. 9. The rate of change of energy of the unstable mode in ITG, explicitly showing calculation of the energy transfer from the unstable to stable mode via zonal flows ($N_{1 \rightarrow 2}$).

and damping terms turned off establishes that the rate of non-conservation of energy due to numerical effects is of order of $10^{-7}\%$ of the zonal flow damping. Since zonal flow damping orders the smallest energy transfer processes tracked in this paper, numerical error does not effect any of the energy transfer rates described above.

The above analysis showing that instability energy is transferred dominantly to the damped mode does not characterize or quantify concomitant energy transfer in wavenumber space. As shown in Fig. 4, the ratio of viscous dissipation, which is active at high wavenumber, to dissipation by stable modes summed over the entire wavenumber range, is smaller than 10%. Most of this wavenumber range is unstable because the high k wavenumber range with $\gamma_1 < 0$ is limited for simulation configurations consistent with earlier work.¹⁴ Hence we have looked at the ratio of energy transfer out of a low k wavenumber range, which is smaller than a quarter of the unstable range, to the rate of dissipation within that range. The ratio remains less than 20%, implying dominant energy transfer is to stable modes within the unstable wavenumber range. We expect that the ratio of energy transferred to high k relative to energy dissipated by damped modes at low k can vary from model to model, with the present simulations yielding very low values. However, the general result that ITG saturation and transport in numerical models is essentially independent of the wavenumber resolution much beyond the instability range indicates that energy dissipation by damped modes in the instability range is significant in all cases.

To further probe this result, we have used bispectral analysis to look at energy transfer between selected wavenumbers, similar to the study done in Ref. 19. This is shown in Fig. 10 which plots the nonlinear transfer function for eigenmodes at different wavenumbers. The exact quantity plotted in Figs. 10(a), 10(b), and 10(d) is

$$N_{1k}(k') = \text{ARe}[C_{1mn}\beta_1^*\beta_m'\beta_n''|_{k'_y \neq 0, k_y} + C_{1Pn}\beta_1^*P_z'\beta_n''|_{k'_y=0} + C_{1mP}\beta_1^*\beta_m'P_z''|_{k'_y=k_y} + C_{1Fn}\beta_1^*v_z'\beta_n''|_{k'_y=0} + C_{1mF}\beta_1^*\beta_m'v_z''|_{k'_y=k_y}], \quad (20)$$

averaged over the saturated state. The terms in the equation are explained in the Appendix. Effectively, it is the sum of nonlinear energy transfer out of/into the unstable mode at wavenumber k via coupling with modes k' and $k-k'$. The quantity shown in Fig. 10(c) is the same except for wherever 1 appears, it is replaced by 2, i.e., the energy transfer out of/into the stable mode at wavenumber k . In Fig. 10, different k 's are chosen and the nonlinear energy transfer spectrum over k' is plotted. Fig. 10(a) is for the unstable mode at $k=(0,0.2)$. It shows a strong coupling with a zonal flow $k'=(-0.08,0)$ and as a result, strong energy transfer to $k-k'= (0.08,0.2)$. In Fig. 10(b), we look at the unstable mode at $k=(0.08,0.2)$. Again it shows strong coupling with the zonal flow at $k'=(-0.08,0)$ to give energy to $k-k'= (0.16,0.2)$. It should be noted that the sign of energy transfer to mode $(0,0.2)$ is still negative, indicating the unstable mode at $(0.08,0.2)$ gives some energy back to the $(0,0.2)$ mode. Taking a look at the nonlinear transfer of the stable

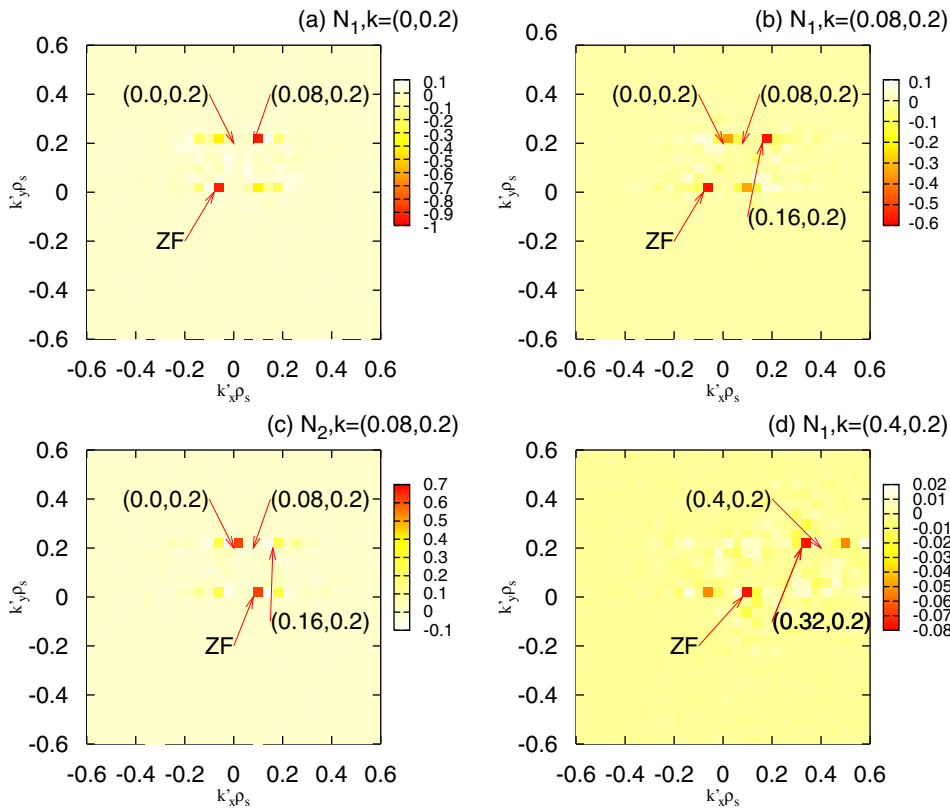


FIG. 10. The nonlinear transfer function spectrum for modes at different wavenumbers.

mode at $k = (0.08, 0.2)$ in Fig. 10(c), we see that it receives energy from mode $(0, 0.2)$. This is most of the energy seen in Fig. 10(a) going from the unstable mode at $(0, 0.2)$ to mode $(0.08, 0.2)$. Thus, the transfer to higher wavenumber is actually transfer to stable modes at higher wavenumber. Fig. 10(d) shows nonlinear transfer for a high wavenumber $(0.4, 0.2)$ that is still in the unstable range. The magnitude of nonlinear transfer has reduced by more than a factor 10 compared to Fig. 10(a). This is because at every step of energy transfer to higher wavenumber, significant energy is lost to the stable modes.

We turn now to the question of how zonal flows and stable modes are initially excited. In the linear stage, both zonal flows and stable modes are damped and their amplitudes decrease. At the beginning of the nonlinear stage, both of these are excited by parametric excitation, i.e., by the beating of two unstable modes at different wavenumbers.⁶ This stage corresponds to the large overshoot of fluctuation level typically observed in simulations.^{15,16} Once the zonal flow and stable modes reach a finite amplitude, the stable branch is maintained at a finite amplitude by nonlinearly coupling with both the unstable modes and zonal flows. At the same time, the zonal flow is pumped by both the unstable and stable modes. This stage corresponds to the saturated phase of the simulations. Both stages are shown in Fig. 11. In this figure, the rate of change of energy of the stable mode is divided by the energy of the stable mode, giving a nonlinear growth rate. Just as before, the growth rate is classified into the different coupling terms. For example, γ_{11} is defined as $N_{211}/(\sum_{k_y \neq 0} (1 + k^2 + |R_2|^2) |\beta_2|^2)$, where N_{211} is the coupling of the stable mode with 2 unstable modes. N_{211} is defined like N_{111} except that the unstable mode at k is

replaced by a stable mode. Similarly, $\gamma_{(12+21)}$ represents coupling with one unstable and one stable mode, and γ_{22} represents coupling with two stable modes. $\gamma_{ZP(F)}$ represents coupling with zonal pressure(flow). From $t = 0$ up to $t = 100L_n/c_s$, the stable mode is seen to be excited by coupling with two unstable modes. After $t = 100L_n/c_s$, the coupling with one zonal flow and one unstable mode is seen to dominate. The peak growth rate occurs at $t = 12L_n/c_s$. If we look at the energy of the stable mode, it initially decays because it is linearly damped but then increases due to nonlinear coupling. Its steepest growth occurs at $t = 12L_n/c_s$, corresponding to the peak nonlinear growth rate in Fig. 11.

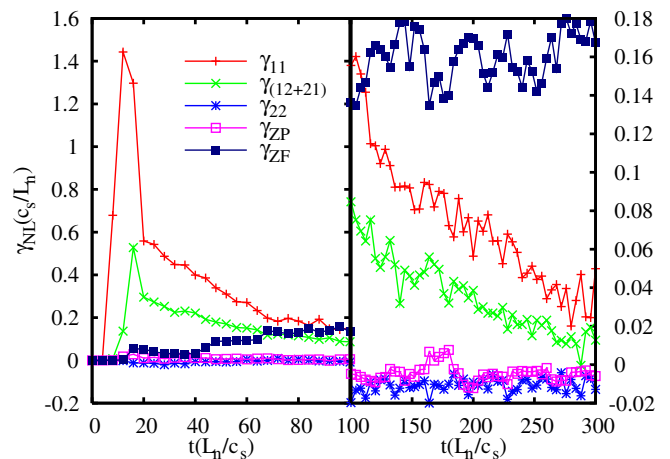


FIG. 11. The nonlinear growth rate of the stable modes derived from the different nonlinear couplings of the stable mode which are similar to Eq. (17). The second panel is a continuation of the first panel with the y axis magnified and x axis shrunk.

We have looked at the energy dynamics of the stable modes, and they show a similar and consistent result. The stable modes are also seen to couple primarily with the unstable modes, with the zonal flows acting as a mediator.

IV. ENERGY TRANSFER IN TRIADS INVOLVING ZONAL MODES

We examine why energy transferred from unstable to stable modes through triads involving a zonal flow as a mediator is the preferred energy transfer channel. Consider the dominant transfer rate $N_{1F2} + N_{12F}$. From the Appendix,

$$N_{12F} = \sum_{k_y \neq 0} 2(1 + k^2 + |R_1|^2) Re \left[\left(\frac{1}{R_1 - R_2} \right) \left(\frac{-i}{2} \right) \times \sum_{k'_y = k_y} k_y \left[R'_2 + \frac{R_2(k''^2 - k'^2)}{(1 + k^2)} \right] \langle \beta_1^* \beta_2' v_z'' \rangle \right], \quad (21)$$

where N_{1F2} has the same form with $''$ and $'$ interchanged. Like all transfer rates, N_{12F} is governed by a triplet correlation of mode amplitudes and a coupling coefficient. The coupling coefficient is $k_y [R'_2 + R_2(k''^2 - k'^2)/(1 + k^2)]$. The angle brackets of the triplet correlation $\langle \beta_1^* \beta_2' v_z'' \rangle$ indicate that N_{12F} is part of an equation that was averaged by multiplication with a complex conjugate. The triplet correlation has amplitude and phase information, and the latter in particular contributes critically to the magnitude of N_{12F} . We show that correlations like $\langle \beta_1^* \beta_2' v_z'' \rangle$ and $\langle \beta_1^* \beta_2' p_z'' \rangle$, in which one member is a zonal field and the other members are a stable and unstable mode, have the smallest frequency sum and hence the longest interaction time of all possible energy transfer triplets. We then show that transfer rates involving a zonal flow (N_{12F}) are larger than transfer rates involving a zonal pressure (N_{12P}) by virtue of the relative magnitudes of amplitudes and coupling coefficients.

A. Triplet phase

The correlation $\langle \beta_1^* \beta_2' v_z'' \rangle$ is governed by an evolution equation that is derived from Eqs. (11) and (12). Starting from $d \langle \beta_1^* \beta_2' v_z'' \rangle / dt = \langle \dot{\beta}_1^* \beta_2' v_z'' \rangle + \langle \beta_1^* \dot{\beta}_2' v_z'' \rangle + \langle \beta_1^* \beta_2' \dot{v}_z'' \rangle$, we substitute for $\dot{\beta}_1^*$, $\dot{\beta}_2'$ and \dot{v}_z'' from Eqs. (11) and (12) (transposed to the appropriate wavenumber). The result is

$$\left\{ \frac{d}{dt} + i[\omega_F'' + \omega_2' - \omega_1^*] \right\} \langle \beta_1^* v_z'' \beta_2' \rangle = \mathcal{G}, \quad (22)$$

where $\omega_F'' = \omega_1|_{k'_y=k_y} = -i\nu$ (for the ITG case). The nonlinearity \mathcal{G} is constructed by multiplying the right hand side of the complex conjugate of Eq. (11) written for β_1^* by $\beta_2' v_z''$ and adding to similar constructs from the right hand sides of Eqs. (11) and (12) for $\dot{\beta}_2'$ and \dot{v}_z'' , respectively. As such, each term of \mathcal{G} is proportional to quartic correlations. Note that Eq. (22) is part of the standard correlation hierarchy in turbulence in which the evolution equation of any correlation is governed by a nonlinearity comprised of correlations of the next higher order. The equation cannot be solved analytically to reveal its amplitude and phase dependence without some

sort of closure. The simulation results, which will be detailed shortly, are well described by closures such as eddy damped quasi normal Markovian (EDQNM).²⁰ In EDQNM, part of \mathcal{G} is proportional to $\langle \beta_1^* \beta_2' v_z'' \rangle$ and renormalizes the complex triplet frequency to $\hat{\omega}_F'' + \hat{\omega}_2' - \hat{\omega}_1^* = \omega_F'' + \omega_2' - \omega_1^* + \Delta\omega_F'' + \Delta\omega_2' - \Delta\omega_1^*$, where $\Delta\omega_j$ ($j = 1, 2$, or F) is a nonlinear (amplitude-dependent) complex frequency. In the rest of \mathcal{G} , which we label $\hat{\mathcal{G}}$, the quartic correlations are expressed as products of two quadratic correlations. Equation (22) can be formally integrated to yield

$$\langle \beta_1^* \beta_2' v_z'' \rangle = \exp\{-i[\hat{\omega}_F'' + \hat{\omega}_2' - \hat{\omega}_1^*]t\} \times \int_0^t \exp\{i[\hat{\omega}_F'' + \hat{\omega}_2' - \hat{\omega}_1^*]t'\} \hat{\mathcal{G}} dt'.$$

In the steady state, $\hat{\mathcal{G}}$ varies on a slower time scale than $[\hat{\omega}_F'' + \hat{\omega}_2' - \hat{\omega}_1^*]^{-1}$, yielding

$$\langle \beta_1^* \beta_2' v_z'' \rangle = \frac{\hat{\mathcal{G}}}{i[\hat{\omega}_F'' + \hat{\omega}_2' - \hat{\omega}_1^*]}. \quad (23)$$

In this form, the frequency mismatch $[\hat{\omega}_F'' + \hat{\omega}_2' - \hat{\omega}_1^*]$ is clearly the inverse lifetime of the triplet correlation and $\hat{\mathcal{G}}$ is the component of the correlation that carries the dependencies on coupling coefficients and amplitudes in the form of products of quadratic correlations. For a given $\hat{\mathcal{G}}$, when the lifetime is longer, the correlation and N_{1F2} are larger.

We, therefore, examine the value of $\hat{\omega}_F'' + \hat{\omega}_2' - \hat{\omega}_1^*$, starting first with the linear component $\omega_F'' + \omega_2' - \omega_1^*$. In this triad $k-k'$ is a zonal wavenumber, i.e., $k'_y = k_y$. Both k and k' are nonzonal wavenumbers so that $\delta = 1$ in ω_1^* and ω_2' . Also, since most of the energy is concentrated in wavenumbers smaller than unity, we can assume that $k^2 \leq \nu, \chi \ll 1$, and $(\delta + k^2) = 1 + O(\nu)$. Then, $\omega_F'' = -i\nu$, $\omega_2' = k_y/2 - ik_y[(1 + \eta)\epsilon]^{1/2} + O(\nu)$, $\omega_1^* = k_y/2 - ik_y[(1 + \eta)\epsilon]^{1/2} + O(\nu)$, and $\omega_F'' + \omega_2' - \omega_1^* = O(\nu)$. If we consider $\langle \beta_1^* \beta_2' p_z'' \rangle$, we also have $\omega_F'' + \omega_2' - \omega_1^* = O(\nu)$. However, it is easily verified that any other combination of a zonal frequency and two nonzonal frequencies, or of three nonzonal frequencies yields a frequency mismatch that is order unity instead of order $\nu \ll 1$. Note too that if the zonal flow damping rate is order unity, the frequency mismatch also becomes order unity instead of small. Large ν removes an efficiency of energy transfer by shortening the interaction time, therefore requiring larger amplitudes to match the instability energy input rate. This mechanism by which zonal flow damping affects turbulence level is a very different effect than the idea that large ν kills the zonal flow and its capacity to suppress turbulence via shear.

These analytical predictions can be verified by looking at the frequency mismatch of exact roots of the dispersion relation calculated by the simulation. The wavenumber k is arbitrarily selected as $(-0.08, 0.2)$. Then a scan is done over k' to see for which triads $(k, k', k-k')$ the frequency mismatch is minimum. In doing this, several combinations of stable and unstable modes are tested. A triad involves a zonal mode whenever k'_y is either 0.0 or 0.2. First, we look at $|\omega_1^* + \omega_2' + \omega_1''|$. This is a triad involving three unstable modes. If $k'_y = 0.0$,

then ω'_1 is taken as $-i\nu$, which is the zonal flow damping. If $k'_y = 0.2$, then ω''_1 is taken as $-i\nu$. This is because of Eq. (7) which shows that the unstable mode maps to the zonal flow. The scan over k' is shown in Fig. 12(a). It shows a minimum value in the regions near k'_y values of 0.0 and 0.2. The exact minimum value is 0.139 at $k' = (1.0, 0.0)$, which is a zonal flow. Next, we consider $|\omega_1^* + \omega_2' + \omega_1''|$. This involves sum of two unstable modes and one stable mode. For $k'_y = 0$, $\omega_2' = -i\chi k'^4$, following Eq. (8). For $k'_y = k_y$, $\omega_1'' = -i\nu$. The scan over k' is shown in Fig. 12(b). Again the minimum lies near $k'_y = 0.2$ which represents coupling to a zonal flow. The exact minimum value of the frequency mismatch is 0.0016 at $k' = (0.04, 0.24)$. This is not a zonal mode coupling but close to it. The frequency mismatch for the mode $k' = (0.0, 0.2)$ is 0.01. We can also combine two stable modes and one unstable mode, $|\omega_1^* + \omega_2' + \omega_2''|$. If $k'_y = 0$, then $\omega_2' = -i\chi k'^4$. If $k'_y = k_y$, then $\omega_2'' = -i\chi k'^4$. This shows minimum frequency mismatch for a range of k'_y going from 0.0 to 0.2, as displayed in Fig. 12(c). The minimum value is 0.0007 at $k' = (-0.2, 0.0)$ and $k' = (0.12, 0.20)$. These observations show that the frequency mismatch is minimum for triads involving a zonal field or modes close to a zonal wavenumber.

The linear frequency mismatch is only part of the correlation time of triplet correlations, except in weak turbulence situations where the nonlinear frequencies are negligible. We now consider the frequency mismatch with the nonlinear frequencies $\Delta\omega_j$. The nonlinear frequencies can be calculated from the closure (see, for example, Ref. 21), but we opt here to extract them directly from simulation data as done in Ref. 22. For each eigenmode for each wavenumber, the frequency spectrum is calculated. A Lorentzian can be fitted to this frequency spectrum. The position of the peak of the Lorentzian gives the real part of $\hat{\omega} = \omega + \Delta\omega$, whereas its width gives the imaginary part. The sign of the imaginary part is chosen depending on whether it is an unstable or stable mode. In this way, the nonlinearly broadened frequencies are calculated and used instead of the linear frequencies for calculation of frequency matching.

We again consider the three cases done for the linear eigenfrequencies. For $|\omega_1^* + \omega_1' + \omega_1'' - \Delta\omega_1^* + \Delta\omega_1' + \Delta\omega_1''|$, a similar scan is done in k' with k again chosen as

$(-0.08, 0.2)$. The frequency sum is plotted against k'_y for $k'_x = 0$ in Fig. 13(a). The minimum value is 0.083 at $k'_y = 0.12$. However, this is not a triad with a zonal mode. For $|\omega_1^* + \omega_2' + \omega_1'' - \Delta\omega_1^* + \Delta\omega_2' + \Delta\omega_1''|$, the result is similar to the linear phase calculation. As shown in Fig. 13(b), the minimum frequency mismatch occurs again at $k'_y = 0.2$, and its value is 0.029. This is a coupling with a zonal mode (at $k-k'$) and a stable mode (at k'), and its phase mismatch is less than half of the minimum mismatch for $|\omega_1^* + \omega_1' + \omega_1'' - \Delta\omega_1^* + \Delta\omega_1' + \Delta\omega_1''|$. This shows that the mismatch is smaller for triads that involve one zonal mode, one unstable, and one stable mode, compared to one zonal mode and two unstable modes. For $|\omega_1^* + \omega_2' + \omega_2'' - \Delta\omega_1^* + \Delta\omega_2' + \Delta\omega_2''|$, the result is shown in Fig. 13(c). Using only linear phases, this quantity showed minimum mismatch for triads involving zonal modes as well as a range of non-zonal triads between $k'_y = 0.0$ and $k'_y = 0.2$. But using the nonlinear phases, we see minimum mismatch only for triads involving zonal modes, i.e., at $k'_y = 0.0$ where the mismatch is 0.003 and at $k'_y = 0.2$, where the mismatch is 0.03.

These results show that the frequency mismatch is minimum for triads involving an unstable mode, a stable mode, and a zonal mode. Such triads are the dominant nonlinear coupling terms, leading to saturation. Moreover, as stated before, the minimum value of the frequency mismatch scales with ν , the zonal flow damping. This is because the flow damping rate (times i) is the zonal mode frequency in the linear frequency mismatch. This is displayed in Table I, which shows that the frequency mismatch of a triad containing an unstable mode, a stable mode, and a zonal flow scales with the zonal flow damping rate. However, we can also consider zonal mode triads in which the pressure damping is used for the zonal mode frequency. The pressure damping is χk^4 so the triads would become $|\omega_1^* + \omega_2' - i\chi k^4|$. The same cancellation occurs as explained above and a zonal mode triad can be approximated as χk^4 . Since χ is of the order of ν and $k < 1$, the zonal pressure triads would also show a very small value of the frequency sum just like the zonal flow triads, indicating minimum frequency mismatch. As a result, low frequency mismatch does not explain why zonal flow triads are more important than zonal pressure triads.

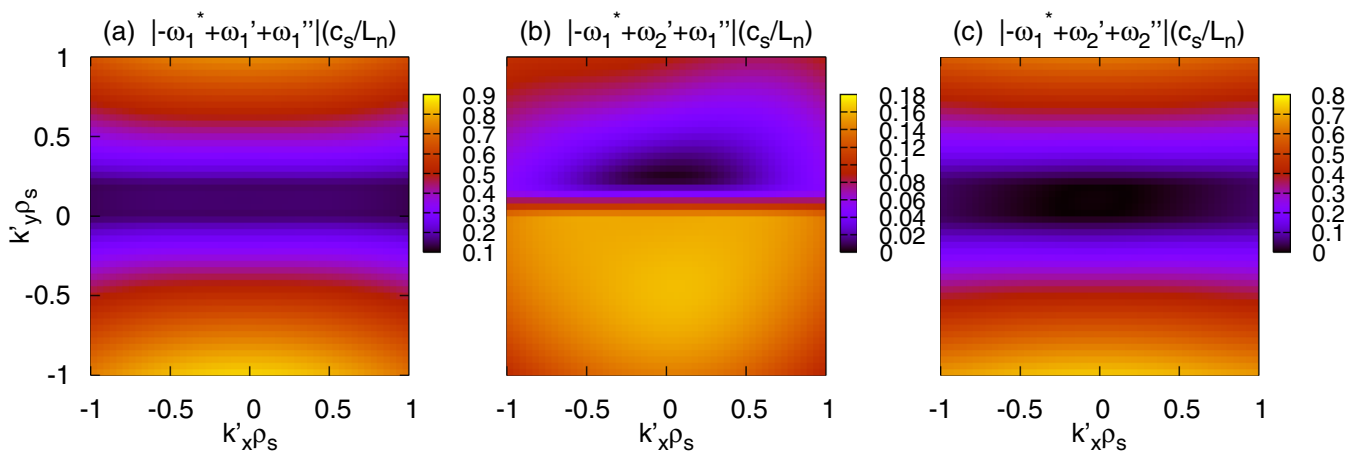


FIG. 12. The frequency sum using linear frequencies, $|\omega_1^*(k) + \omega_j(k') + \omega_l(k-k')|$ for $k = (-0.08, 0.2)$.

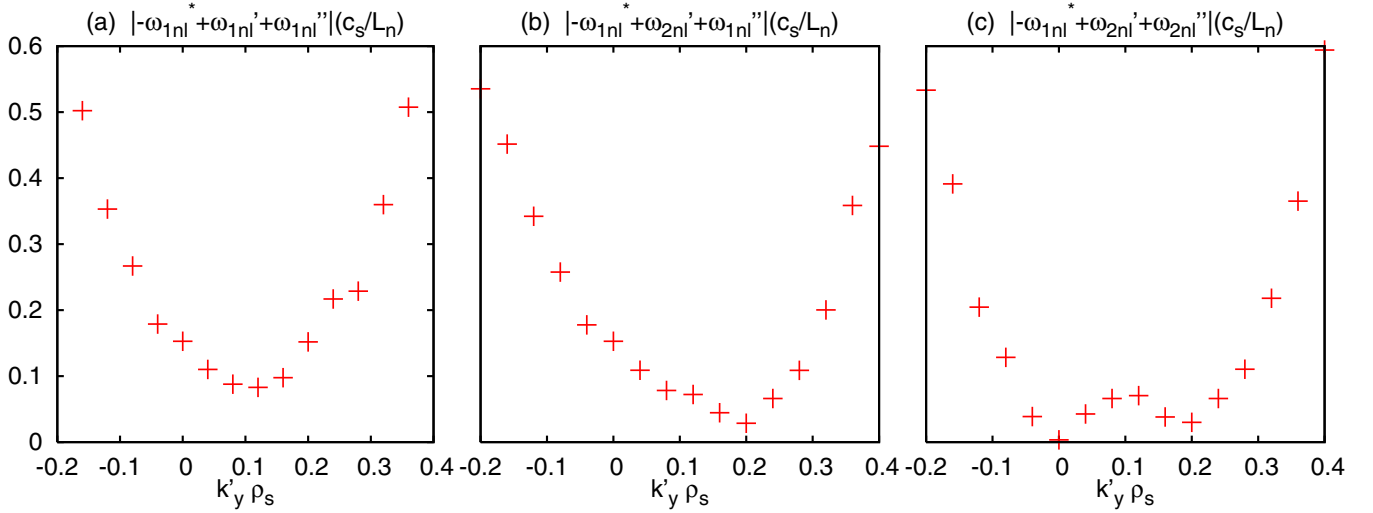


FIG. 13. The frequency sum using the nonlinear frequencies, $|-\omega_i^*(k) + \omega_j(k') + \omega_l(k - k') - \Delta\omega_i^*(k) + \Delta\omega_j(k') + \Delta\omega_l(k - k')|$ for $k = (-0.08, 0.2)$.

B. Coupling coefficients

We examine now the coupling coefficients in the triplet nonlinear terms of the energy equations. We have already identified the coupling coefficient in N_{12F} , prior to discussing in detail its phase. We consider other triplet terms in the evolution equations for the energies $(1 + k^2 + |R_1|^2)|\beta_1|^2$, $(1 + k^2 + |R_2|^2)|\beta_2|^2$, $|p_k|^2$, and $(\delta + k^2)|\phi_k|^2$. The coupling coefficient in each triplet term is equal to the product of either $1 + k^2 + |R_i|^2$ (for non-zonal modes) or unity (for zonal modes) and a corresponding coupling coefficient from the eigenmode evolution equations, Eqs. (11)–(13). Each coupling coefficient in Eq. (11) contains a factor $1/(R_1 - R_2)$. For long wavelengths ($k^2 \ll 1$), $(R_1 - R_2) \approx -2i[(1 + \eta)/\epsilon]^{1/2}$, independent of k . Also, for long wavelengths, the eigenvector magnitudes $|R_1|, |R_2|$ lie within the range of 6–7 and they vary weakly with k . Thus, the factors $(1 + k^2 + |R_i|^2)$ are roughly constant. The remaining part of the coupling coefficients is strongly dependent on k , and the power of k indicates magnitude, with smaller powers representing stronger coupling. In analyzing the power, we do not distinguish between k and k' , but treat both as comparably smaller than unity. The following wavenumber dependence is found for the coupling coefficients in the evolution equations of the unstable and stable modes [Eq. (11)]:

$$\begin{aligned} C_{lmn}(\text{or } N_{lmn}) &\sim k^2, \\ C_{lFn}(\text{or } N_{lFn}) &\sim C_{lmF}(\text{or } N_{lmF}) \sim k, \\ C_{lPn}(\text{or } N_{lPn}) &\sim C_{lmP}(\text{or } N_{lmP}) \sim k^2, \end{aligned} \quad (24)$$

where $l, m, n = 1$ or 2 . The strongest coupling coefficients are with the zonal flows ($\sim k$). But this holds for both the

ETG and ITG cases. The coupling coefficients in the evolution equation of the zonal pressure [Eq. (13)] are

$$C_{Pmn}(\text{or } N_{Pmn}) \sim k^2. \quad (25)$$

The coupling coefficients in the evolution equation of the zonal flow [Eq. (12)] are

$$C_{Fmn}(\text{or } N_{Fmn}) \sim \frac{k^5}{\delta + k^2}. \quad (26)$$

This shows that the coupling coefficients for the zonal flows are stronger for the ITG case ($\sim k^3$) compared to the ETG case ($\sim k^5$). This is part of the reason why zonal flows are excited to a higher level in the ITG case. However, as explained above [Eq. (24)], the unstable mode coupling with zonal flows is stronger than its coupling with other modes for both ETG and ITG cases. Hence, this alone cannot explain the difference between the two cases. Consequently, we must consider relative amplitude information, which also contributes to the magnitude of the nonlinear transfer.

C. Amplitude of zonal modes

The strength of a triad also depends on the amplitudes of the three fields in it. We compare the zonal pressure and zonal flow amplitudes in the ETG and ITG cases. The energy level of the zonal flow and zonal pressure averaged over the saturated state are provided in Table II. The level of zonal pressure is more than zonal flow in both cases. In the ETG case, the zonal flow is smaller than zonal pressure by a factor of 15. However, in the ITG case, the zonal flow is only 3 times smaller than the zonal pressure. This is possibly due to the fact that the nonlinear coupling coefficients of the zonal flow field are stronger in ITG case compared to ETG case.

The three main points of this section can be summarized as follows. (1) Triplet frequency matching favors triads that include a zonal mode, an unstable mode, and a stable mode, in both ETG and ITG. (2) Coupling coefficients in the unstable mode energy evolution equation favor zonal flow triads over zonal pressure triads, in both ETG and ITG. (3)

TABLE I. Frequency sum for $k = (-0.08, 0.2)$ and $k' = (0.0, 0.2)$.

| ν | $ -\omega_1^*(k) + \omega_2(k') + \omega_1(k - k') $ |
|-------|--|
| 0.01 | 0.0104 |
| 0.02 | 0.0203 |
| 0.05 | 0.0503 |

TABLE II. Zonal field energy levels.

| | ETG | ITG |
|-------------------------|--------------------|--------------------|
| $\langle p_z^2 \rangle$ | 1.17×10^4 | 5.75×10^2 |
| $\langle v_z^2 \rangle$ | 5.60×10^1 | 6.10×10^1 |

Amplitude favors zonal pressure triads over zonal flow triads in ETG but gives relatively equal weightage to both in ITG. These three facts combined together explain why in ITG the saturation happens with a triad involving the unstable mode, a zonal flow, and a stable mode, as shown explicitly in Sec. III.

V. CONCLUSIONS

The interaction of zonal flows with ITG turbulence involves damped modes, making the process different from prior descriptions. We show that zonal flows mediate energy transfer from the unstable mode to a damped mode in the large-scale wavenumber range of the instability. Direct energy transfer to damped modes without zonal-flow mediation is less efficient, and when zonal flows are artificially removed, it requires higher amplitudes to match the energy injection rate of the instability.

After an initial transient phase in which zonal flows and the damped mode are each driven by beating wavenumbers of the unstable mode, the dominant energy transfer is through a 3-wave interaction between the unstable mode, the zonal flow, and the stable mode. Of the net energy transferred from the unstable mode, almost all (more than 99%) ends up in the stable mode, where it is dissipated. The very small amount of energy that ends up in the zonal flow (less than 1%) is balanced by the small zonal flow damping. The triplet interaction of an unstable mode, a zonal flow, and a stable mode forms the dominant energy transfer channel through a combination of three factors. Its three-wave nonlinear frequency mismatch is minimum, leading to the largest nonlinear interaction time. It has the largest coupling coefficient. This triplet is also enhanced in ITG relative to ETG by a larger zonal flow amplitude and a smaller zonal pressure amplitude.

This process deviates from the standard picture of zonal flow effects in ITG turbulence in several ways. Saturation is achieved at low k through the damped mode, which has not been considered in the standard picture. With the damped mode, the amount of energy dissipated at high k is not large nor is the amount of energy transferred to high k . Consequently zonal flow shear, frequently invoked to explain the effect of zonal flows on turbulence, while an active process, is not a significant player in the saturation or energy transfer physics in the simulations described here. The ratio of energy transferred to high k relative to energy dissipated at low k may vary with other models. Zonal-flow drive in the steady state is dominated by the triad of the unstable mode, the zonal flow, and the damped mode. Descriptions of zonal flow excitation that do not include damped modes miss the dominant saturation process.

There is considerable evidence that the processes described here for a reduced fluid model also operate in gyrokinetic models of ITG turbulence. The primary difference is that instead of a single damped mode, there are many damped modes.³ However, it remains true that saturation is caused by damped modes in the same wavenumber range as the instability, that nonlinear transfer to these modes dominates transfer to high k , and that zonal flows participate in the three-wave interactions that take instability energy to the damped modes.²³ The interaction of zonal flows and damped modes in gyrokinetics will be described in detail elsewhere. One unexpected result from gyrokinetics is that the strongest damped mode excited is a tearing parity mode that makes the magnetic field stochastic and causes magnetic-fluctuation induced electron thermal transport.^{23,24} This mode is excited by the same triad coupling of an unstable mode, a zonal flow, and a stable mode as described in this paper. Hence while mediating a reduction of ion channel transport by lowering the fluctuation level, the zonal flow mediates an *enhancement* of electron channel transport. This is not an optimal situation for confinement. However, the role of zonal flows in mediating energy transfer to damped modes raises the intriguing possibility that it may be possible to externally manipulate the dominant energy transfer through fluctuations other than zonal flows and thereby control to which type of damped mode most of the energy flows. This could then be used to select for a desirable or optimal set of transport properties.

ACKNOWLEDGMENTS

The authors acknowledge useful conversations with David Hatch and David Newman. This work was supported by the U.S. Department of Energy Grant DE-FG02-89ER53291.

APPENDIX: NOTATIONS, EXPRESSIONS, AND SYMBOLS

The nonlinear coupling coefficients for Eq. (11) are

$$C_{lmn} = \frac{(-1)^{l-1}}{(R_1 - R_2)} \frac{(\mathbf{k}' \times \hat{z} \cdot \mathbf{k})}{2} \left[R'_m - R''_n + \frac{R_{3-l}(k''^2 - k'^2)}{(1 + k^2)} \right], \quad (\text{A1})$$

$$C_{lFn} = \frac{(-1)^{l-1}}{(R_1 - R_2)} \frac{(-ik_y)}{2} \left[R''_n - \frac{R_{3-l}(k''^2 - k'^2)}{(1 + k^2)} \right], \quad (\text{A2})$$

$$C_{lPn} = \frac{(-1)^{l-1}}{(R_1 - R_2)} \frac{(-k'_x k_y)}{2}, \quad (\text{A3})$$

$$C_{lMf} = \frac{(-1)^{l-1}}{(R_1 - R_2)} \frac{(-ik'_y)}{2} \left[R'_m + \frac{R_{3-l}(k''^2 - k'^2)}{(1 + k^2)} \right], \quad (\text{A4})$$

$$C_{lMf} = \frac{(-1)^{l-1}}{(R_1 - R_2)} \frac{(-k'_y k'_x)}{2}. \quad (\text{A5})$$

The nonlinear coupling coefficients for the zonal flow equation [Eq. (12)] are

$$C_{Fmn} = \frac{-ik'_y k_x^2 (k''^2 - k'^2)}{2(\delta + k_x^2)}. \quad (\text{A6})$$

The nonlinear coupling coefficients for the zonal pressure equation [Eq. (13)] are

$$C_{Pmn} = \frac{(k'_y k_x)}{2} (R'_m - R''_n). \quad (\text{A7})$$

Here $l, m, n = 1$ or 2 and $\mathbf{k}'' = \mathbf{k} - \mathbf{k}'$, $R_{1,2} = R_{1,2}(k)$, $R'_{1,2} = R_{1,2}(k')$ and $R''_{1,2} = R_{1,2}(k'')$. The terms in Eq. (15) are

$$Q_u = \sum_{k_y \neq 0} -2k_y (1 + \eta + \epsilon) \text{Im}(R_1) |\beta_1|^2, \quad (\text{A8})$$

$$Q_s = \sum_{k_y \neq 0} -2k_y (1 + \eta + \epsilon) \text{Im}(R_2) |\beta_2|^2, \quad (\text{A9})$$

$$Q_{us} = \sum_{k_y \neq 0} -2k_y (1 + \eta + \epsilon) \text{Im}(R_1 \beta_1 \beta_2^* + R_2 \beta_1^* \beta_2), \quad (\text{A10})$$

$$D = \sum_{k_y \neq 0} -2\chi k^4 |p_k|^2 - 2\nu k^2 |\phi_k|^2, \quad (\text{A11})$$

$$D_{zonal} = \sum_{k_y = 0} -2\chi k^4 |p_k|^2 - 2\nu k^2 |\phi_k|^2. \quad (\text{A12})$$

The three wave coupling terms in Eq. (17) are

$$N_{1mn} = \sum_{k_y \neq 0} \mathcal{A} \text{Re} \left[\sum_{k'_y \neq 0, k_y} C_{1mn} \beta_1^* \beta'_m \beta''_n \right], \quad (\text{A13})$$

$$N_{1Pn} = \sum_{k_y \neq 0} \mathcal{A} \text{Re} \left[\sum_{k'_y = 0} C_{1Pn} \beta_1^* P'_z \beta''_n \right], \quad (\text{A14})$$

$$N_{1mP} = \sum_{k_y \neq 0} \mathcal{A} \text{Re} \left[\sum_{k'_y = k_y} C_{1mP} \beta_1^* \beta'_m P''_z \right], \quad (\text{A15})$$

$$N_{1Fn} = \sum_{k_y \neq 0} \mathcal{A} \text{Re} \left[\sum_{k'_y = 0} C_{1Fn} \beta_1^* v'_z \beta''_n \right], \quad (\text{A16})$$

$$N_{1mF} = \sum_{k_y \neq 0} \mathcal{A} \text{Re} \left[\sum_{k'_y = k_y} C_{1mF} \beta_1^* \beta'_m v''_z \right], \quad (\text{A17})$$

where $\mathcal{A} = 2(1 + k^2 + |R_1|^2)$. The three wave coupling terms in the zonal field energy Eqs. (18) and (19) are

$$N_{Pmn} = \sum_{k_y = 0} 2\text{Re} \left[\sum_{k'_y \neq 0} C_{Pmn} P'_z \beta'_m \beta''_n \right], \quad (\text{A18})$$

$$N_{Fmn} = \sum_{k_y = 0} 2\text{Re} \left[\sum_{k'_y \neq 0} C_{Fmn} v'_z \beta'_m \beta''_n \right], \quad (\text{A19})$$

where in Eqs. (A13)–(A19), $m, n = 1$ or 2 .

¹K. D. Makwana, P. W. Terry, J.-H. Kim, and D. R. Hatch, *Phys. Plasmas* **18**, 012302 (2011).

²J.-H. Kim and P. W. Terry, *Phys. Plasmas* **17**, 112306 (2010).

³D. R. Hatch, P. W. Terry, F. Jenko, F. Merz, and W. M. Nevins, *Phys. Rev. Lett.* **106**, 115003 (2011).

⁴G. Berkooz, P. Holmes, and J. L. Lumley, *Annu. Rev. Fluid Mech.* **25**, 539 (1993).

⁵P. W. Terry, D. A. Baver, and S. Gupta, *Phys. Plasmas* **13**, 022307 (2006).

⁶R. Gatto, P. W. Terry, and D. A. Baver, *Phys. Plasmas* **13**, 022306 (2006).

⁷P. W. Terry, D. A. Baver, and D. R. Hatch, *Phys. Plasmas* **16**, 122305 (2009).

⁸Z. Lin, T. S. Hahm, W. W. Lee, W. M. Tang, and R. B. White, *Science* **281**, 1835 (1998).

⁹P. H. Diamond, S.-I. Itoh, K. Itoh, and T. S. Hahm, *Plasma Phys. Controlled Fusion* **47**, R35 (2005).

¹⁰P. H. Diamond, S. Champeaux, M. Malkov, A. Das, I. Gruzinov, M. N. Rosenbluth, C. Holland, B. Wecht, A. I. Smolyakov, F. L. Hinton, Z. Lin, and T. S. Hahm, *Nucl. Fusion* **41**, 1067 (2001).

¹¹T. S. Hahm, M. A. Beer, Z. Lin, G. W. Hammett, W. W. Lee, and W. M. Tang, *Phys. Plasmas* **6**, 922 (1999).

¹²C. Holland, G. R. Tynan, R. J. Fonck, G. R. McKee, J. Candy, and R. E. Waltz, *Phys. Plasmas* **14**, 056112 (2007).

¹³P. W. Terry, *Rev. Mod. Phys.* **72**, 109 (2000).

¹⁴C. Holland, P. H. Diamond, S. Champeaux, E. Kim, O. Gurcan, M. N. Rosenbluth, G. R. Tynan, N. Crocker, W. Nevins, and J. Candy, *Nucl. Fusion* **43**, 761 (2003).

¹⁵T.-H. Watanabe, H. Sugama, and S. Ferrando-Margalet, *Nucl. Fusion* **47**, 1383 (2007).

¹⁶A. M. Dimits, W. M. Nevins, D. E. Shumaker, G. W. Hammett, T. Danert, F. Jenko, M. J. Pueschel, W. Dorland, S. C. Cowley, J. N. Leboeuf, T. L. Rhodes, J. Candy, and C. Estrada-Mila, *Nucl. Fusion* **47**, 817 (2007).

¹⁷P. W. Terry, *Phys. Rev. Lett.* **93**, 235004 (2004).

¹⁸R. A. Moyer, G. R. Tynan, C. Holland, and M. J. Burin, *Phys. Rev. Lett.* **87**, 135001 (2001).

¹⁹M. Nakata, T.-H. Watanabe, and H. Sugama, *Phys. Plasmas* **19**, 022303 (2012).

²⁰M. Lesieur, *Turbulence in Fluids* (Kluwer Academic, Norwell, 1990).

²¹D. A. Baver, P. W. Terry, R. Gatto, and E. Fernandez, *Phys. Plasmas* **9**, 3318 (2002).

²²P. W. Terry and W. Horton, *Phys. Fluids* **26**, 106 (1983).

²³D. R. Hatch, M. J. Pueschel, F. Jenko, W. M. Nevins, P. W. Terry, and H. Doerk, *Phys. Rev. Lett.* **108**, 235002 (2012).

²⁴E. Wang, W. M. Nevins, J. Candy, D. Hatch, P. Terry, and W. Guttenfelder, *Phys. Plasmas* **18**, 056111 (2011).